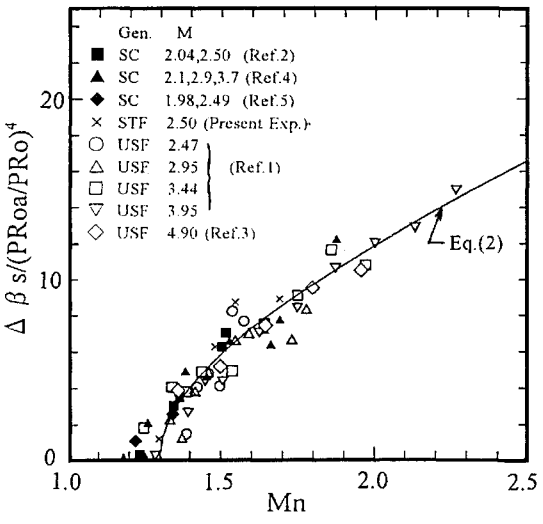

Fig. 4 Improved correlation of the separation angles in terms of overall pressure rise.

deg, and $2.0 \leqq M \leqq 3.5$, the value of PR_{oa} has been shown to be accurately predicted using the equation

$$PR_{oa} = \pi PR_{os}[-0.06865 + 0.2189\xi + 0.2803\xi^2 - 0.05|M - 2.5|(\pi/2 - \xi)]/(2\xi) \quad (1)$$

where PR_{os} is the two-dimensional oblique shock pressure ratio based on a flow-deflection angle of α (cf., PR_o is the shock pressure ratio based on β_o) and ξ is $\tan^{-1}[1/(\sin\alpha \tan\lambda)]$ (in radians; see Fig. 1c). Equation (1) provides values within 3% of the corresponding CFD values.

Each group of data shown in Fig. 3 can be expressed by a hyperbolic function, with each function having a vertex at about 1.3 (intersection between the function and the abscissa of Fig. 3). The angle $\Delta\beta_s$ appears to be approximated by $c_1 M_n^b (M_n^2 - 1.3^2)^{1/2}$, where c_1 is a constant and the power b, which varies with the fin geometry, is 0 for USF and nearly 1 for SC. Using Taylor–Maccoll theoretical values, PR_{oa} for SC has been shown to correlate with $M_n^{2.25}$, and M_n^2 is directly related to PR_o. Hence, PR_{oa}/PR_o is on the order of $M_n^{2.25}/M_n^2 = M_n^{0.25}$. By dividing $\Delta\beta_s$ by $(PR_{oa}/PR_o)^4$, in the case of SC, the hyperbolic function can be simplified as $\Delta\beta_s/(PR_{oa}/PR_o)^4 \sim c_1 M_n (M_n^2 - 1.3^2)^{1/2}/(M_n^{0.25})^4 = c_1(M_n^2 - 1.3^2)^{1/2}$. As shown in Fig. 4, the parameter $\Delta\beta_s/(PR_{oa}/PR_o)^4$ has caused not only SC data but also STF data to approach that of the USF group. Finally, the relationship

$$\Delta\beta_s/(PR_{oa}/PR_o)^4 = 7.8\sqrt{M_n^2 - 1.3^2} \quad (2)$$

(depicted by the solid line in Fig. 4) has been employed to predict the separation angles β_s. The separation angles β_s predicted by Eq. (2) has been shown to be fairly accurate [within 2 deg (1 deg) of the corresponding experimental value for nearly 90% (70%) of the data points in Fig. 4]. This method can provide a rapid and reasonable estimation of the location of primary separation.

Acknowledgment

The authors would like to express their sincere gratitude to F. K. Lu for providing data from tests conducted by himself and his colleagues.

References

[1]Lu, F. K., and Settles, G. S., "Mach Number Effects on Conical Surface Features of Swept Shock-Wave/Boundary-Layer Interactions," *AIAA Journal*, Vol. 28, No. 1, 1990, pp. 91–97.

[2]Deng, X. Y., and Liao, J. H., "Correlation of Conical Interactions Induced by Sharp Fins and Semicones," *AIAA Journal*, Vol. 31, No. 5, 1993, pp. 962, 963.

[3]Rodi, P. E., and Dolling, D. S., "An Experimental/Computational Study of Sharp Fin Induced Shock Wave/Turbulent Boundary Layer Interactions at Mach 5: Experimental Results," AIAA Paper 92-0749, Jan. 1992.

[4]Avduyevskiy, V. S., and Gretsov, V. K., "Investigation of a Three-Dimensional Separated Flow Around Semicones Placed on a Plane Plate," NASA TTF-13578, July 1971.

[5]Saida, N., Ooka, T., and Koide, S., "Interaction Between Shock Waves and Boundary Layer Induced by a Semicone Placed on a Flat Plate," *Journal of the Japan Society for Aeronautical and Space Sciences*, Vol. 33, No. 374, 1985, pp. 159–166 (in Japanese).

[6]Saida, N., Ogata, R., and Koide, S., "Shock Wave/Boundary Layer Interactions Induced by a Rhombic Delta Fin," *Proceedings of the Symposium on Shock Waves*, edited by R. Yamane, Tokyo Inst. of Technology, Tokyo, Japan, 1996, pp. 51–54 (in Japanese).

[7]Koide, S., Griesel, C. J. W., and Stollery, J. L., "Correlation of Shock Angles Caused by Rhombic Delta Wings," *AIAA Journal*, Vol. 34, No. 7, 1996, pp. 1529–1531.

[8]Koide, S., Griesel, C. J. W., and Stollery, J. L., "Effects of Strakes on a Glancing Shock Wave/Turbulent Boundary-Layer Interaction," *Journal of Aircraft*, Vol. 32, No. 5, 1995, pp. 985–992.

Visualization and Analysis of Bow Shocks in a Superorbital Expansion Tube

Margaret Wegener,* Tim McIntyre,†
Halina Rubinsztein-Dunlop,‡ Alexis Bishop,§
Ray Stalker,¶ and Richard Morgan**
University of Queensland, Brisbane 4072, Australia

Nomenclature

M	= Mach number
β	= angle of shock to freestream flow
γ	= ratio of specific heats
δ	= angle included between model and shock
ρ	= density
1	= upstream of shock
2	= downstream of shock

Introduction

SUPERORBITAL expansion tubes are being developed at the University of Queensland to generate flows faster than Earth orbital speeds.[1] They are capable of producing enthalpies far greater than those of existing ground-based testing facilities (free piston-driven shock tunnels and conventional expansion tubes), which enables the aerodynamic study of vehicles designed to return to Earth's atmosphere or enter the atmosphere of other planets.

Accompanying the development of these facilities is the requirement for reliable instrumentation capable of performing measurements within the short test times, typically up to 100 μs. Optical techniques offer this capability, providing nonintrusive measurements recorded over submicrosecond laser pulse durations. One well-established diagnostic method is interferometry, which records gas density variations over the whole field of view in a manner that can be interpreted both qualitatively and quantitatively. A relatively new form is holographic interferometry. In an early practical application to gas dynamics, holographic interferometry was used to study supersonic air flow around cones in a wind tunnel, as described

Received Nov. 20, 1995; accepted for publication Feb. 19, 1996.

*Postgraduate Student, Department of Physics and Department of Mechanical Engineering.

†Research Fellow, Department of Physics.

‡Associate Professor, Department of Physics.

§Postgraduate Student, Department of Physics.

¶Professor, Department of Mechanical Engineering. Associate Fellow AIAA.

**Associate Professor, Department of Mechanical Engineering. Member AIAA.

by Tanner.[2] More recent examples of its application include measurements made of flow around various models at low Mach numbers for comparison with computational fluid dynamics (CFD),[3] and in a high enthalpy shock tunnel.[4]

Reported here are the first optical measurements of very high enthalpy flows in a superorbital expansion tube. Holographic interferograms have been recorded of air flows at a velocity of 11 km s^{-1} around a variety of models. The ratios of densities across the shocks have been calculated from measurement of the shock shapes displayed in the interferograms. These results have been compared with predictions based on assumptions of frozen and equilibrium flow.

Experiment

The test flow was produced in the superorbital expansion tube, X1. This facility is a triple diaphragm expansion tube with compound driver consisting of a free piston primary driver and shock-heated secondary driver section. The principles of its operation have been described by Neely and Morgan.[1]

The equilibrium freestream conditions of the flow used were calculated, indicating a specific enthalpy of 86 MJ kg^{-1} (or equivalent flight speed of 13 km s^{-1}), a density of 2.8×10^{-3} kg m^{-3}, and a Mach number of 5.6. The speed of the shock in the tube ahead of the model was measured to be 11.1 km s^{-1}. Because of the manner in which the tunnel generates the flow, oxygen is fully dissociated in the freestream while nitrogen has a dissociation fraction of 0.50. Two asymmetric wedges were used to produce flow deflections of 15, 20, 23, and 32 deg, and a cylinder was used to examine the shock standoff distance.

Double exposure holographic interferograms were recorded using the 532-nm output of a pulsed, injection seeded Nd:YAG laser with a pulse length of approximately 10 ns and linewidth of 0.005 cm^{-1} to ensure temporal and spatial coherence. Two-dimensional integrated images were recorded using plane wave illumination of the test section. An infinite fringe interferogram provides fringe shifts that are directly proportional to the integrated gas density. To perform fringe analysis effectively, a reference pattern of carrier fringes has been introduced by tilting one of the wave fronts between exposures. A computer-operated timing system, triggered by a pressure transducer upstream of the test section, was used to fire the laser. Photodiodes monitoring the flow luminosity and the laser pulse were used to verify that a hologram was recorded within the test flow duration of approximately 50 μs and after the establishment of steady flow. Flow luminosity was removed by the use of a narrow-band filter and an aperture. The holograms were recorded on Kodak® 120-01 plates and later reconstructed using a He-Ne laser.

A selection of the results of the experiments is shown in Figs. 1 and 2. These reconstructed holographic interferograms indicate a uniform freestream, as shown by the parallelism of the fringes ahead of the shock front. Figure 1 is an image of the flow over one of the wedges, in which oblique shocks attached to the tip of the model can be identified by sharp bends in the fringes. Behind the shock the flow also appears relatively uniform, although there may be some nonuniformity for the larger angle. Figure 2 shows the flow over a cylinder with its curved bow shock. Across the shock one observes a small sharp fringe jump. Immediately behind, the fringes reverse direction before undergoing a second change close to the body. The size of these shifts decreases away from the centerline of the flow. The first reversal can be attributed to the liberation of electrons caused by collisions initiated behind the shock front. Little evidence of fringe shift reversal is observed for flow over the wedges indicating that the temperature is insufficient to cause significant ionization in these cases. The second fringe reversal is thought to be due to heat transfer in the thermal boundary layer and/or radiation losses. A similar effect has been observed in ionizing argon flows over a cylinder.[5]

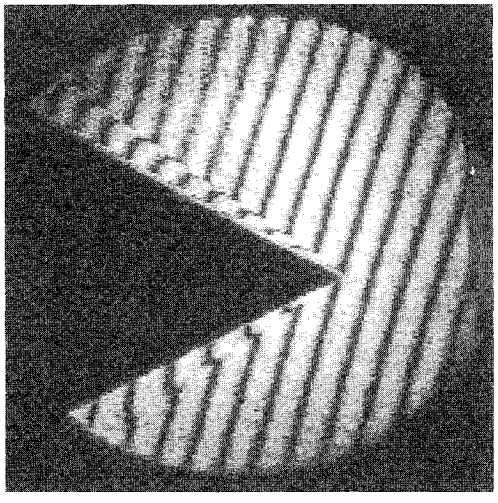

Fig. 1 Holographic interferogram of a wedge-shaped model causing flow to be deflected by 32 deg on the upper side and 23 deg on the lower side; flow is from right to left.

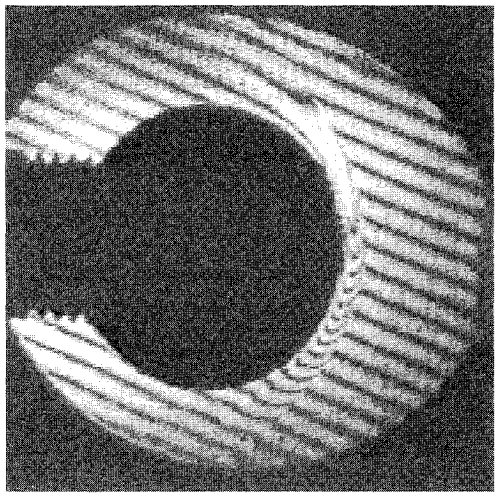

Fig. 2 Holographic interferogram of the flow around a cylindrical model; flow is from right to left.

The determination of total density from the fringe shift is complicated by the presence of electrons. Unlike other particles, the refractive index for electrons is strongly dependent on wavelength. Thus, it is possible to measure total density and electron density by recording interferograms at two separate wavelengths. This will be necessary to quantify the effects of ionization occurring in flows over blunt bodies at these high velocities.

Analysis

Assuming the flow to be quasi-two dimensional, the density ratio across the shock (the ratio of the density immediately behind the shock to the freestream density) was derived from the interferograms. It also was calculated from predictions in the limits of frozen and equilibrium flow.

In the analysis of the experimental results for the wedges, the density ratio was obtained from the basic expression relating the densities and the geometry of the model and flow (for example, see Ref. 6):

$$\rho_2/\rho_1 = \tan\beta/\tan\delta \tag{1}$$

where the shock angle was measured over the whole field of view. Uncertainties in the density ratios were propagated from uncertainties in the measurement of the angles.

For frozen flow predictions, the shock relationship for a perfect gas (for example, see Ref. 6):

$$\frac{\rho_2}{\rho_1} = \frac{(\gamma+1)M_1^2 \sin^2\beta}{(\gamma-1)M_1^2 \sin^2\beta + 2} \tag{2}$$

was used with values of γ and M_1 from equilibrium freestream predictions to obtain the density ratio across the shock for the complete range of β.

For equilibrium flow predictions, densities downstream of the shock were calculated from the equation of state using equilibrium

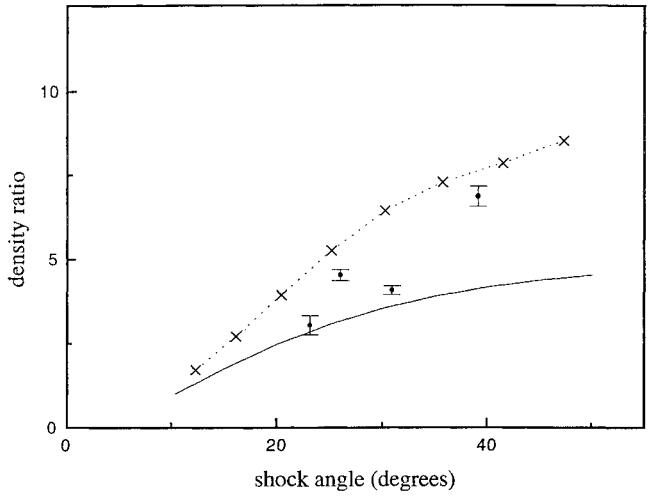

Fig. 3 Variation of density ratio across the shock with shock angle: •, experimental data; ——, frozen predictions; and ×, equilibrium predictions.

predictions of thermodynamic parameters, and compared with similarly predicted upstream density, for a variety of shock angles.

The variation of the density ratio with shock angle is plotted in Fig. 3. As would be expected, density ratio tends to increase with increasing shock angle. The experimental data lie between the values predicted from ideal and equilibrium calculations. This supports the validity of the computed freestream conditions.

For the cylinder, the shock standoff distance normalized by the cylinder radius was measured to be 0.13. A correlation given by Hornung[7] for flow over blunt bodies was used to predict a standoff distance from the density jump across the shock. This value was calculated to be 0.47 for perfect gas conditions and 0.21 for equilibrium, both being significantly larger than that measured. A number of possible reasons for this have been considered. First, Hornung's correlation was developed for a dissociating nitrogen gas flow. The difference between correlations for nitrogen and air can be expected to be unimportant. However, the partially dissociated freestream and the presence of electrons behind the bow shock may influence the accuracy of the correlation in this case. Second, the assumption of two dimensionality may not be valid for the model used. Comparison of the cylinder dimensions (diameter 20 mm and length 25 mm) confirms that three-dimensional effects may be significant. Deviation from two dimensionality results in a curvature of the shock along the direction of the cylinder axis and a reduction in the standoff distance. Hornung's correlation for a cylinder would then overpredict the shock standoff distance. A third possibility is the influence of radiation cooling. At the high velocities existing in the flow, extremely high temperatures can be expected, at which radiative losses would lead to a lowering of the density and hence shock standoff distance. The importance of each of these effects on the shock standoff for the cylinder is to be the subject of future experimentation.

Conclusions

Good quality interferograms of superorbital air flow around a range of models have been recorded holographically. From the images, shock angles and standoff distances have been measured. The results for flow over the wedges gave density ratios that lie within expected limits. However, the shock standoff distance for the cylinder was found to be smaller than expected and a number of explanations have been proposed.

The results discussed here represent the initial measurements obtainable from holographic interferometry. Considerably more information about the density field around models is to be extracted by more detailed analysis of these results and extension to three-dimensional imaging.

Acknowledgments

This work was supported by the Australian Research Council. Thanks are extended to Henry Lorek for design of the timing system and to Ian Johnston for performing equilibrium CFD calculations.

References

[1]Neely, A. J., and Morgan, R. G., "The Superorbital Expansion Tube Concept, Experiment and Analysis," *Aeronautical Journal*, Vol. 98, No. 973, 1994, pp. 97–105.

[2]Tanner, L. H., "A Holographic Interferometer and Fringe Analyzer, and Their Use for the Study of Supersonic Flow," *Optics and Laser Technology*, Vol. 4, No. 6, 1972, pp. 281–287.

[3]Spring, W. C., Yanta, W. J., Gross, K., and Lopez, C. A., "The Use of Holographic Interferometry for Flow Field Diagnostics," *New Trends in Instrumentation for Hypersonic Research*, edited by A. Boutier, Kluwer Academic, Dordrecht, The Netherlands, 1993, pp. 97–112.

[4]Eitelberg, G., Fleck, B., and McIntyre, T. J., "Holographic Interferometry on the High Enthalpy Shock Tunnel in Göttingen," AGARD:ARW, 1992.

[5]Hornung, H. G., and Sandeman, R. J., "Interferometric Measurements of Radiating Ionizing Argon Flow over Blunt Bodies," *Journal of Physics D: Applied Physics*, Vol. 7, No. 6, 1974, pp. 920–935.

[6]Liepmann, H. W., and Roshko, A., *Elements of Gasdynamics*, Wiley, New York, 1957, p. 87.

[7]Hornung, H. G., "Non-equilibrium Dissociating Nitrogen Flow over Spheres and Circular Cylinders," *Journal of Fluid Mechanics*, Vol. 53, Pt. 1, 1972, pp. 149–176.

Accurate Numerical Integration of State–Space Models for Aeroelastic Systems with Free Play

Mark D. Conner,* Lawrence N. Virgin,† and Earl H. Dowell‡
Duke University, Durham, North Carolina 27708-0300

Nomenclature

A_i	= state–space coefficient matrix for the ith linear subdomain
$a, c, r_\alpha, r_\beta, x_\alpha, x_\beta, \mu, \omega_\alpha, \omega_\beta, \omega_h$	= typical section parameters as defined in Ref. 2
b	= semichord
$f_n(\,)$	= functional representation for the nth state
h_0	= initial plunge displacement
U	= freestream velocity
U_f	= linear flutter velocity
x_D	= additional dummy state variable used for Henon integration
x_n	= nth system state
α, β, h	= pitch, flap, and plunge displacements, respectively
$\zeta_\alpha, \zeta_\beta, \zeta_h$	= modal damping coefficients
$(\dot{})$	= velocity in the given degree of freedom

Introduction

THE general form of the equations of motion for the three-degree-of-freedom aeroelastic typical section in two-dimensional, incompressible flow was derived by Theodorsen.[1,2] Edwards et al.[3] proposed a state–space model for this linear system incorporating a two-state approximation to Theodorsen aerodynamics to determine the unsteady aerodynamic loads. However, similar state–space models for piecewise linear systems, such as those with free play in the structural stiffness of one or more degrees of freedom,

Received Aug. 21, 1995; revision received Feb. 15, 1996; accepted for publication Feb. 15, 1996.

*Graduate Research Assistant, Department of Mechanical Engineering and Materials Science.

†Associate Professor of Mechanical Engineering, Department of Mechanical Engineering and Materials Science. Member AIAA.

‡J. A. Jones Professor and Dean, School of Engineering, Department of Mechanical Engineering and Materials Science. Fellow AIAA.